Determination of Threshold Pressure for Infiltration of NaCl Preforms by a Zinc Base Alloy and its Effect on Young´s Modulus by Numerical Simulation

JORGE E. RIVERA-SALINAS, KARLA M. GREGORIO-JÁUREGUI,
ALEJANDRO CRUZ-RAMÍREZ, JOSÉ A. ROMERO-SERRANO,
EDUARDO RAMÍREZ-VARGAS, VÍCTOR H. GUTIERRÉZ-PÉREZ,
and LUIS F.J. HERNÁNDEZ-QUINTANAR

The capillary infiltration of the Zn-22Al-2Cu (Zinalco) alloy into NaCl packed particles of sizes 496, 687, and 945 μm was studied using centrifugal casting. The threshold pressure for infiltration of NaCl particles with Zinalco was deduced experimentally, which increased as the diameter of the particles decreased. The work of immersion was determined from the threshold pressure with a value of 2.1. The infiltration proceeded at distinctly different rates for the three particle sizes studied. An equation to predict the threshold pressure to infiltrate Zinalco alloy into NaCl particles for given particle size and volume fraction was established. The micromechanical analysis showed that the strength of the foam depended strongly on the level of infiltration of the derived foam. As the level of infiltration increased, the stress distribution in the foams produced became homogeneously distributed in all the struts that make up the cell, which increases the strength of foam. The elastic modulus of the as-produced Zinalco foams is governed by structural parameters such as the pore size and the strut length. Thinner and shorter struts in the foam increase its ability to resist elastic deformation in the foam.

I. INTRODUCTION

OPEN-CELL metal foams are materials with an optimum combination of mechanical properties such as high specific strength, energy absorption, and electrical/thermal conductivity among others at minimum weight, whose functionality makes them suited to be used in a

JORGE E. RIVERA-SALINAS is with the Catedrático CONACyT – Departamento de Procesos de Transformación. Centro de Investigación en Química Aplicada – CIQA, 25294, Saltillo, Coahuila, Mexico. Contact e-mail: enrique.rivera@ciqa.edu.mx. KARLA M. GREGORIO-JÁUREGUI, ALEJANDRO CRUZ-RAMÍREZ, and JOSÉ A. ROMERO-SERRANO are with the Departamento de Ingeniería en Metalurgia y Materiales, Instituto Politécnico Nacional, Escuela Superior de Ingeniería Química e Industrias Extractivas – ESIQIE, UPALM, 07738, Mexico D.F., Mexico. EDUARDO RAMÍREZ-VARGAS is with the Departamento de Procesos de Transformación. Centro de Investigación en Química Aplicada – CIQA, 25294, Saltillo, Coahuila, Mexico. VÍCTOR H. GUTIERRÉZ-PÉREZ is with the Departamento de Formación Profesional Específica. Instituto Politécnico Nacional - Unidad Profesional Interdisciplinaria de Ingeniería campus Zacatecas (UPIIZ). 98160, Zacatecas, Mexico. LUIS F. J. HERNÁNDEZ-QUINTANAR is with the Academia de Ciencias de la Ingeniería, UPIIH-Instituto Politécnico Nacional, 42162, Hidalgo, Mexico.

Manuscript submitted April 22, 2020; accepted November 23, 2020.
Article published online January 3, 2021

wide range of applications.[1,2] An economical and efficient route to fabricate open-cell metal foams is replication processing, which consists of infiltrating liquid metals into porous preforms packed by salt particulates. In this process, salt particulates are commonly used because they are leachable in solvent or water; moreover, the morphology and size of packed particulates can be controlled.[3] Once the composite or specimen is cooled, the NaCl preform is dissolved to leave an open-cell metal foam.

An important factor affecting the replication process is the poor wetting of salts by molten metals. Most metallic melts exhibit poor wettability on ceramics and ionic solids such as sodium chloride, which can impede the infiltration from being spontaneous.[4–6] Nevertheless, using pressure to drive the liquid into the salts overcomes this problem; therefore, it is necessary to create a pressure drop through the liquid by external pressure to aid the driving of the metal into the interstices of the porous preform. Full infiltration can be achieved only if the minimum pressure drop in the liquid metal is equal to the capillary pressure drop, which is considered the threshold pressure. If the pressure in the liquid metal is higher than the threshold pressure, the rate of infiltration is higher. The pressure infiltration determines the formation of struts which in

turn influence the mechanical properties of the foam. Thus, pressure infiltration is a means of controlling foam density.[7] However, pressure infiltration must be controlled to avoid compressive deformation and cracking of the porous preform.[8] Over-infiltration produced by high infiltration pressure also causes encapsulation of several NaCl particles by the metal, preventing the water to leach the NaCl out,[9] as well as the infiltration of defects on the surface of the NaCl particles. The latter is a kind of infiltration of defects, which produces small finger-like protrusions.[6,10] X-ray microtomographic three-dimensional views of the structure of pure Al replicated foams made with NaCl preforms infiltrated at pressures of 0.1 MPa (relative density 76.4 pct) and 15.5 MPa (relative density 74.7 pct) show that after lower pressure infiltration the foam structure is relatively neat and regular; with higher pressures it is more irregular, featuring more plates between cell walls, together with a series of metal fingers that extend into the pores.[10] Depending on the intended applications of the foam, the formation of these protrusions at higher infiltration pressures reduces their effectiveness as a functional material; it affects the properties of infiltration of the foams by reducing their permeability.[6] On the other hand, it was found that increasing the applied pressure and hence the foam relative density, causes a steady increase in Young's modulus of the foams, which can be attributed to the filling of narrow interparticle gaps.[6]

Some of the routes used to perform liquid infiltration include pressureless/pressure infiltration method and direct squeeze casting (mechanical pressure). However, the productivity of these processes is often low.[11,12] For instance, in the pressureless/pressure infiltration method, the fabrication temperature and production time of the materials are higher and longer, respectively, than those of other fabrication methods, which may allow for undesirable interfacial reactions between the particle and molten metal. Moreover, the main disadvantage of this process is that the melting of the metal and the heating of the preform takes place inside the pressure chamber so that the pressure chamber is a bottleneck for mass production, resulting in low productivity generally.[12–14]

On the other hand, the direct squeeze casting process is particularly prone to extrusion segregation in webs and corners. Macrosegregation has a significant effect on the mechanical properties of the final cast part as well as on the productivity of this process. In addition, machining operations are required to remove the defects which in turns it makes necessary a larger casting to allow for the machining,[15–17] and additional machining operations call for longer durations of production.

Another way to generate pressure indirectly in the molten metal using a relatively simple experimental set up is by centrifugal force.[11,18] In this process, a mold containing a preform is rotated. A relatively small amount of molten metal in the runner is necessary (to avoid a large amount of scrap metal), moreover, the pressure driving the infiltration is relatively low.[12] Studies have shown that liquid infiltration using centrifugal force is a feasible process for producing functionality graded materials,[12,19,20] metal matrix composites,[11] and open-cell metal foams.[21,22] The centrifugal casting process provides sufficient pressure to obtain a full infiltration. Hence, the materials produced using this route meet the requirements in terms of mechanical performance.[11,12,19–22] In addition, this route is considered to be easy, cost-effective, and flexible for the fabrication of parts.[19,20]

Determination of the minimum pressure required for infiltration to occur for a given particle size and volume fraction is a prerequisite to systematically achieve full infiltration and better quality of the foam. Hence, an equation to calculate the threshold pressure for infiltration to occur was derived from the capillary law assuming spherical particles by Mortensen et al.[4]:

$$P_{th} = -6\gamma Cos\theta \frac{V_p}{d_p(1 - V_p)} \quad [1]$$

where P_{th} is the threshold pressure, γ is the surface tension of the alloy, V_p is the volume fraction of the preform, θ is the contact angle and d_p is the diameter of the spherical particles.

The Brooks and Corey semi-empirical model describes the extent of filling (S), which is defined as saturation of the preform with liquid as a function of the applied pressure (P):

$$S = 1 - \left(\frac{P_o}{P}\right)^\lambda \quad [2]$$

where P_o is the bubble pressure, similar to the threshold pressure, and λ is pore size distribution index, which is related to the microscopic geometry of the pores within the preform.[23] The pore size distribution index λ, is determined from the slope of the log-log plot using Eq. [2]. Moreover, the extent of filling in the preform can be characterized indirectly in the porous medium/infiltrant system at hand by a scaling factor (φ), which is used to convert the curves of Hg saturation as a function of the pressure to the infiltration of the same preform by another metal at hand[23]:

$$\varphi = \frac{\gamma^{\text{metal}} \cdot \cos\theta_{\text{metal-preform}}}{\gamma^{\text{Hg}} \cdot \cos\theta_{\text{Hg-preform}}} \quad [3]$$

where γ^{metal} and γ^{Hg} are the surface tension of the metal at hand and Hg, respectively, while $\theta_{\text{metal-preform}}$ and $\theta_{\text{Hg-preform}}$ are the contact angles between the metal, Hg and the preform, respectively. The scaling factor φ is the ratio of the work of immersion in the two systems.

Nowadays, industrial interest is focused on aluminum foams due to the low density and low melting temperature of aluminum alloys. Nevertheless, there are other alloys suitable to produce metallic foams, such as the Zn-Al-Cu alloy named Zinalco, which shows a unique combination of properties such as high strength, good machinability, and low melting point.[21,24] It is important to remark that Zn-Al alloys are receiving considerable attention because they exhibit a good capacity to absorb energy and mechanical damping, which makes them suitable to produce tailored metallic foams. Moreover, the Zn-Al foams find applications in battery

and chemical industries.[25] Notably, manufacturing open-cell metal foams through the replication process using a salt bed that serves as a space holder is an efficient method to produce this kind of foam.[24] The versatility of the method has made it one of the most competitive processes for the production of open-cell foams. As a result, different processing techniques for carrying out the infiltration of Zinalco alloy into NaCl preforms have been explored; in the case of coarse foams with irregular NaCl crystals in the range of 2 to 7 mm, assisted gravity casting was used,[24] mechanical pressure (not specified if gas or piston) for irregular NaCl crystals in the range of 0.84 to 3.90 mm was used,[26] and centrifugal infiltration for spherical crystals in the range of 0.5 to 0.95 mm.[21] The Zinalco foams have a cell size equivalent to NaCl particles.[21,24,26] In the previously mentioned works, the compressive and mechanical properties of the Zinalco foams were investigated. According to these studies, the mechanical strength of the foam can be effectively influenced by the microstructure in the cell-strut of the Zinalco foams as well as the cell sizes. However, it was found that the microstructure of the as-produced samples exhibits a very similar dendritic structure independent of the strut thickness or the salt grain used. Also, it was found that the compressive mechanical properties of the open-cell Zn-Al, as well as the relative density increased when the pore size decreased. With NaCl, fine aluminum foams with an average pore diameter as small as 5 μm can be produced.[27] Though, as the pore size decreases the infiltration of the preform becomes difficult, and systematic approaches are necessary to avoid incomplete or over-infiltration. This research focuses on studying the infiltration process for Zinalco alloy into NaCl preforms. However, intrinsic capillary parameters such as the surface tension γ and the contact angle θ for this and other alloys suitable to produce metallic foams are not reported in the literature. Hence, it is difficult to systematically manufacture metal foams since the available prediction models such as those pointed out above, which allow for achieving optimal control of the process as well as the density of the foam, are defined as a function of the wetting parameters. Furthermore, measuring the dynamic contact angle is a difficult task because it is flow-rate dependent, and it must be measured using infiltration.

Computational fluid dynamics (CFD) analysis of the infiltration process under the actual conditions using a model such as the volume of Fluids (VOF) or the level set method (LSM) for the description of the moving front of infiltration are apt to determine the extent of filling of the preform as a function of the applied pressure (volume forces) when the wettability properties of the system are available. To the best of our knowledge, the contact angle and the surface tension for the system at hand (Zinalco alloy/NaCl preforms) have not been reported in the literature; therefore, a CFD analysis to study infiltration is not a choice. On the other hand, the preparation of open-celled aluminum foams by counter-gravity infiltration casting demonstrates that defects such as insufficient infiltration affect the mechanical properties of the foams.[28] In that work,

it was shown that using the counter-gravity infiltration casting, macro-defect-free aluminum foams with optimal mechanical properties can be produced, which in turn can be used in conjunction with the void content to determine if the main reason why the mechanical properties are affected is due to insufficient infiltration.[28] Following the same argument, the infiltration level of the preform can be assessed indirectly using an alternative way, for example, by drawing on to the micromechanical finite element analysis. The numerical predictions of the elastic modulus of incomplete and fully infiltrated foams should be compared with the experimental value of Young´s modulus of derived foams. According to the closeness of the experimental and numerical compared values, it is possible to determine the level of infiltration.

In the available literature, an estimate of the differential pressure to achieve complete replication of the open pore space left into a NaCl preform by Zinalco alloy has not been reported yet. This parameter of engineering relevance stands out to achieve better quality in the foams, especially if the diameter of the NaCl particles is relatively small. The objective of the current research is to analyze the characteristics of pressure to systematically achieve complete infiltration of Zinalco alloy into NaCl preforms, in addition to presenting practical guidelines for the analysis of the infiltration by centrifugal casting, when intrinsic capillary parameters are not available. To this end, the liquid infiltration of the Zinalco alloy into NaCl particulates with average diameters in the range 496 to 945 μm was investigated to establish the threshold pressure to achieve infiltration. Moreover, the work of immersion and the rates of infiltration are also reported. Liquid infiltration trials were performed under the threshold pressure, and all experiments were carried out in an open atmosphere. The pressure drop in the metal was created by a centrifugal force field, using an experimental setup similar to the references.[10,18] The centrifugation apparatus was designed and constructed. The rate of infiltration was predicted by employing the Washburn's equation,[29] which relates the infiltrated distance as a function of the work of immersion and time, assuming that infiltration is limited by viscous friction. The effects of incomplete infiltration and the strut thickness on the strength of the foam are studied using a 3D micromechanical model of the Zinalco foams.

II. EXPERIMENTAL PROCEDURES

A. *Base Alloy and Spherical Particulates*

A master Zinalco alloy was manufactured by conventional melting in an electric furnace at 540 °C from pure metals. The chemical composition obtained in mass pct was 21.92 Al, 1.81 Cu, and Zn balance.

The as-received NaCl angular particles were melted using a propane gas torch, dispersed by atomized air, and solidified in flight (under atmospheric temperature) as they fell. The manufactured salt particulates retained a spherical shape due to the surface tension force. The

spherical NaCl particles were sieved and classified according to their size. The salt circularity was determined by optical microscopy and the analyzer Image J 4.1 using Eq. [4] shown in Reference 21:

$$\chi = 4\pi\left(\frac{A}{p^2}\right) \qquad [4]$$

where A is the area and p is the perimeter of the particle. Circularity $\chi = 1$ is for a circle.

B. *Zn-22Al-2Cu/NaCl Composites*

The preparation of preforms was carried out by placing the NaCl particles in a stainless steel cylinder of 6 cm internal diameter and 15 cm length. Vibration was applied to the cylinder after adding a small number of particles. This procedure was repeated to ensure efficient packing until the preforms reached a height of 7 cm. Before packing, the inner walls of the cylinder were coated with graphite to facilitate specimen removal. Figure 1 shows the schematic representation of the experimental arrangement used to produce the composites. This arrangement is constituted by two electrical resistance furnaces and a centrifugation system. Both furnaces contain a unit to control the temperature. The system (salt-cylinder) was heated up to a temperature of 600 ± 10 °C for 10 min in an electric furnace. Simultaneously, in another electric furnace, 650 grams of Zinalco alloy was melted at 455 °C, and the temperature was increased up to the pouring temperature of 600 ± 5 °C. Both, the stainless steel cylinder containing the salt preform and the crucible with the molten Zinalco, were extracted from their respective furnaces once the working temperature was reached, and then the molten alloy was poured into the stainless steel cylinder. The cylinder was transferred as quickly as possible into the centrifugation system. Figure 2 shows the centrifugation apparatus designed and constructed, which is constituted by a variable frequency drive, a motor, and a centrifugation chamber that contains two additional stainless steel cylinders that act as a counterweight. The samples were cast using a rotational speed of up to 150 rpm based on the NaCl particle size for 5 min. A metal matrix composite of 6 cm in diameter and 7 cm in height was extracted from the stainless steel cylinder. Cylindrical compression samples were obtained from the as-produce composites, which were 20 mm in diameter and 16.6 mm in height, according to the ASTM E-09 Standard. Later, compression tests were performed using a universal testing machine (Shimadzu 100 kN/10 ft capacity) at a constant crosshead speed of 0.5 mm min^{-1}.

C. *Finite Element Analysis*

For the development of 3D micromechanical models, body-centered (BCC) lattices were built with spheres of diameters 469, 687, and 945 μm, as shown in Figure 3. The strength of the foam produced with a particle size of 469 μm was determined numerically at different levels of infiltration: 85, 90, 95, and 100 pct (Figure 4). Young's modulus of the Zinalco alloy is 20 GPa.[30] Specific details about the numerical methodology for the averaging of stress and strain tensor over the volume of the unit cell, used to predict Young's modulus of the Zinalco foam can be found in.[31] It has been shown in Reference 32 that available closed-form analytical expressions for the prediction of Young's modulus of open-cell foams, such as those of Zue *et al.*[33] (Eq. [5]), Warren and Kraynik[34] (Eq. [6]), and Gant *et al.*[35] (Eq. [7]), overestimate the elastic modulus, whereas the results given by micromechanical finite element analysis are closer to the experimental values.

$$E = \frac{1.009 E_s \rho^2}{1 + 1.514 \rho^2} \qquad [5]$$

$$E = \frac{E_s \rho^2 (11 + 4\rho)}{(10 + 31\rho + 4\rho^2)} \qquad [6]$$

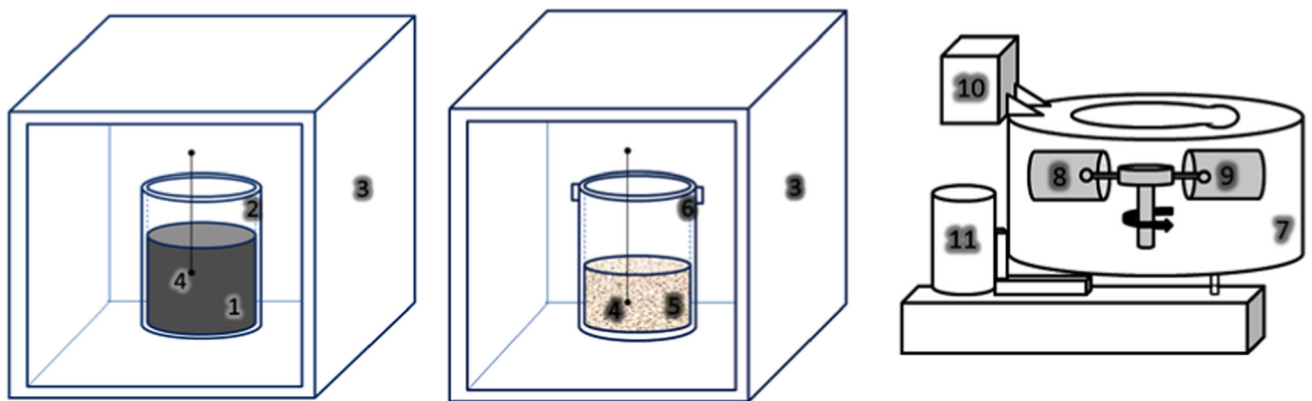$$E = \frac{E_s \rho^2}{1 + 6\rho} \qquad [7]$$

Fig. 1—Schematic of the experimental setup, electrical furnaces, and centrifugation system. (1) Molten metal, (2) SiC crucible, (3) Electrical resistance furnace, (4) Thermocouple, (5) NaCl preform, (6) Stainless steel cylinder, (7) Centrifugation chamber, (8) Counterweight, (9) Molten metal + NaCl preform + Stainless steel cylinder, (10) Variable frequency drive and (11) Motor.
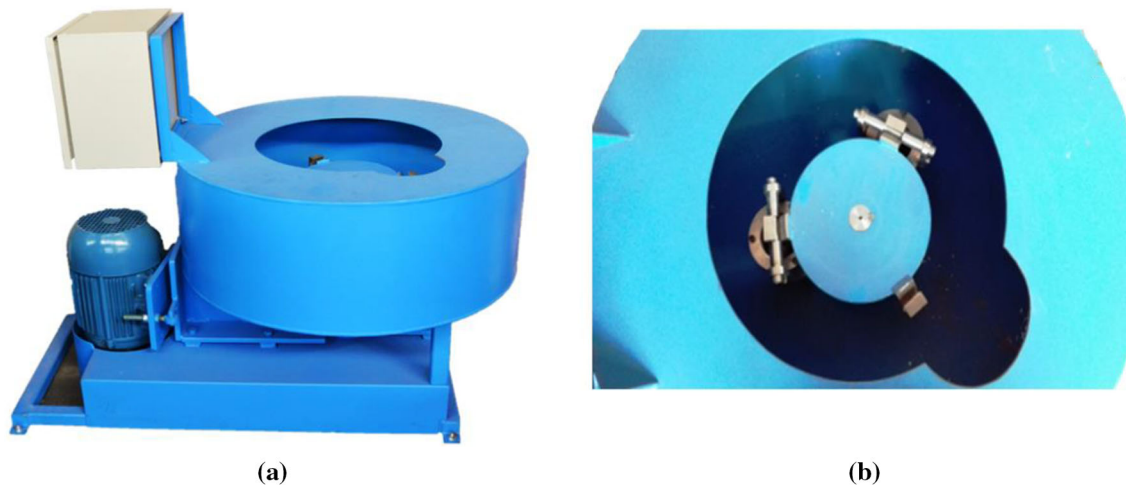
(a)   **(b)**

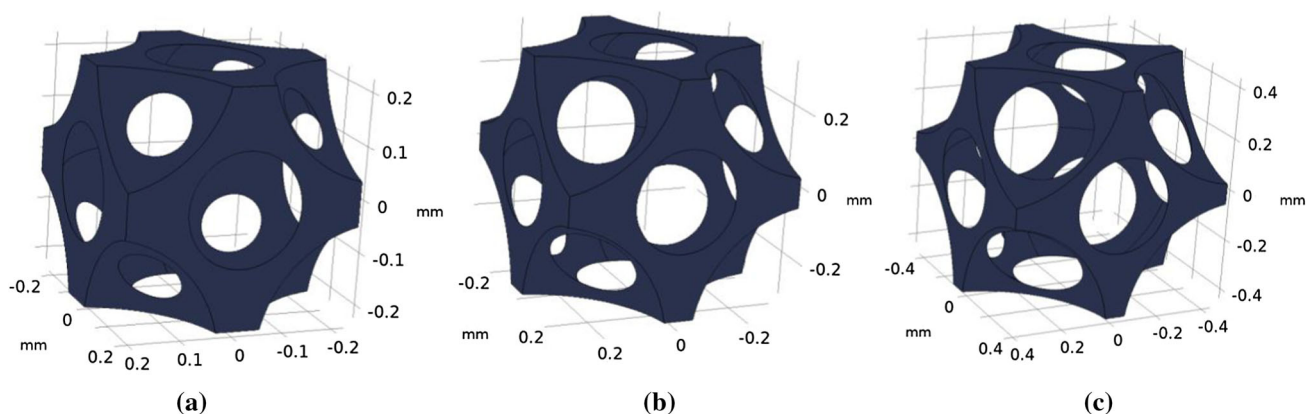Fig. 2—(*a*) Centrifugation apparatus used to produce metal matrix composites and (*b*) its top view.

(a)   **(b)**   **(c)**

Fig. 3—Representation of open-cell foam geometry for the particle size of (*a*) 469 *μ*m, (*b*) 687 *μ*m and (c) 945 *μ*m.

where E_s and ρ are the elastic modulus of the material of the foam and the relative density, respectively. Therefore, if the experimental value of Young's modulus of the foam is compared to the predictions of the analytical models pointed out above, the comparison will suggest that the foam is partially infiltrated, because the models overestimate the elastic modulus. Then, a micromechanical finite element analysis is preferable for the prediction of the elastic modulus of the foams to ensure a proper comparison, as well as to determine how the struts' thicknesses of the foams govern their elastic stiffness. Periodic boundary conditions are prescribed to the lattice or unit cell. The 3D numerical models are developed using the mechanic's module in the software, COMSOL Multiphysics. Mesh refinement is applied to ensure mesh-independent solutions for completely and incompletely infiltrated foams, considering that for the numerical model, it is assumed that the cellular solid is dense with spherical cell morphology. A considerable difference in the comparison of experimental and numerical Young's modulus is attributed to the fact that neither the cellular solid is dense nor the cell morphology is spherical in the experimentally derived

foams, which are common defects that arise during an inadequate infiltration.

III. RESULTS AND DISCUSSION

A. *NaCl Morphology and Particle Size*

The NaCl particulates were classified into three groups after sieving. The average size was determined to be 496, 687, and 945 *μ*m, and their morphology is shown in Figure 5 such as they were produced. The circularity obtained for the NaCl particles based on Equation [4] was 0.94, 0.946, and 0.933 for the sizes of 496, 687, and 945 *μ*m, respectively. According to the circularity obtained, it was concluded that the process used for manufacturing the spherical particles of NaCl allows obtaining satisfactorily round particles.

B. *Zn-22Al-2Cu/NaCl Composites*

In our previous study, Zinalco open-cell foams were successfully prepared using centrifugal casting at 100, 120, and 150 rpm for the particles of sizes 496, 687, and
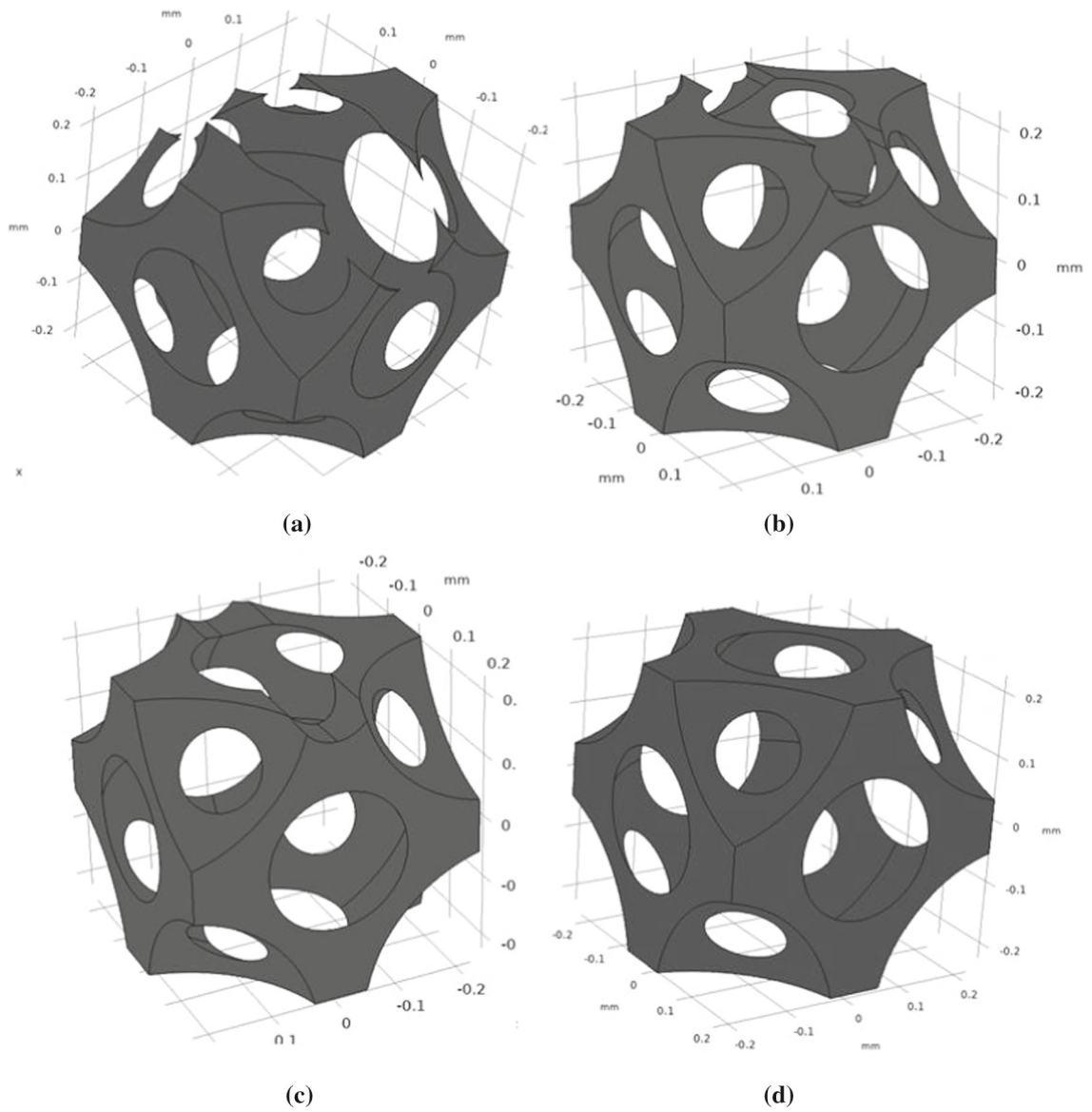
Fig. 4—Representation of open-cell foam for the particle size of 469 μm at different levels of infiltration (*a*) 85 pct, (*b*) 90 pct, (*c*) 95 pct, and (*d*) 100 pct.
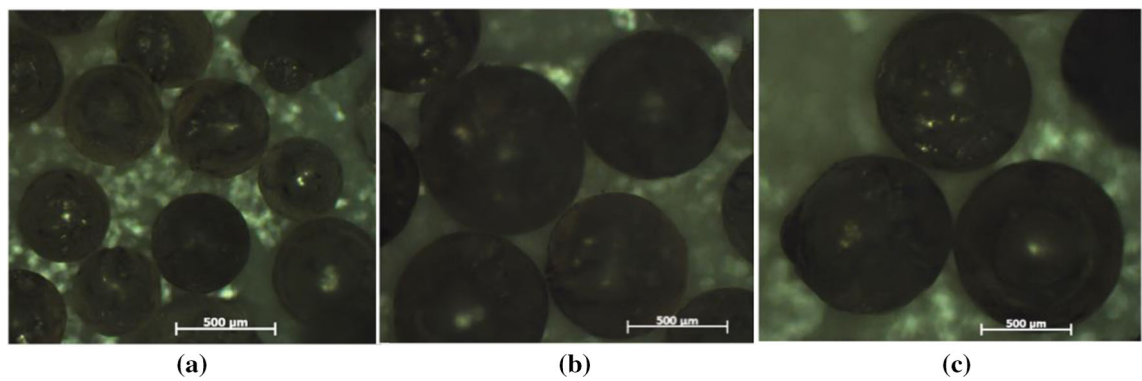

Fig. 5—Photograph of the groups of NaCl particles produced. (*a*) 496 μm, (*b*) 687 μm and (*c*) 945 μm.

945 μm, respectively.[21] In this work, it was found that these rates of rpm produce centrifugal pressures that correspond to the threshold pressures for each particle size, as shown in Section III–C. Three infiltration trials for each particle size were performed for five minutes, and three composites for each particle size were obtained. Images representative of Zinalco/NaCl composites (after the specimens were extracted from the cylinder and they were machined) for the three particle sizes are shown in Figure 6. The as-produced composites were machined to take one sample from each one of them to assess Young´s modulus of the foams obtained after leaching of the salt. The machining of cellular metals is a challenge because the resulting surface is extremely irregular, which leads to tears in the material and surface damage.[36] The bottom part of the sample (a) in Figure 6 shows a noticeable evidence of surface damage caused during the metal-cutting operation, as the damage is on the surface of the machined composite.[36] In Figure 6, it can be observed that all samples had a homogeneous infiltration of the Zinalco alloy into the voids of the preform in the three cases.

Important physical properties to characterize open-cell metal foams are relative density, porosity, and average strut thickness. Because the Zinalco foams produced in this work are prepared exactly under the same technical conditions as in our previous work,[21] in which the characterization of the foams was reported, the foams are not characterized further; however, the experimental results of the foams reported previously[21] with different particle sizes are summarized here in Table I. It can be seen that larger NaCl particles size lead to lower density and relative density of the open-cell Zinalco foams. Hence, smaller NaCl particles size allow to infiltrate more mass of the alloy which

provide increased stiffness as shown in Section III–E. The SEM images of their interconnected structure and the struts of the foams for each particle size can also be found in Reference 21 as well as the images of the as-produced Zinalco/NaCl composites (under the same technical conditions) and cross-sectional images showing homogeneous infiltrations of the NaCl preforms in their longitudinal and transversal directions. In Reference 21, it is shown that the Zn-22Al-2Cu alloy consists of a eutectic microstructure, which shows regions rich in aluminum (α) and zinc (η) phases and the intermetallic (ε) phase corresponding to $CuZn_4$, with a fine inter lamellar structure characterized by regions of α and η phases. Compressive stress-strain curves of Zinalco foams with particle sizes of 496, 687, and 945 μm are shown in Figure 7(a) through (c), respectively. Three samples are considered for each particle size. The stress-strain curves depict three distinct stages as the general trend of stress-strain curves of metal foams: (i) Linear elastic stage, (ii) Flat plateau stage, and (iii) the densification stage. It is observed that the three foam for each particle size exhibit a very similar behavior during compressive deformation, which show that results are consistent during each infiltration trial. The elastic moduli are 0.559, 0.35, and 0.234 GPa for the foams with particle sizes of 496, 687, and 945 μm, respectively. Experimental results of Young's modulus of the Zinalco foams were compared with the numerical predictions to verify if the foams are fully infiltrated, as shown in Section III–E.

C. Threshold Pressure and Centrifugal Pressure

To achieve penetration of molten Zinalco into the body of the NaCl preform, series of experiments were conducted where they were subjected to different speeds of revolution for each particle size to determine the minimum pressure required to achieve complete infiltration (threshold pressure). This was done by varying the rotational speed during the centrifugal casting; the remaining parameters (porosity, temperature, etc.) involved in the process remained constants based on each particle size. To perform the experiments under constant infiltration pressure, the angular velocity was raised as fast as possible up to a fixed value and kept constant. In this work, the driving force for infiltration to occur was the pressure generated by the centrifugal force. Nishida et al.[8] introduced a relationship between the revolution number and the fluid pressure which acts on the preform surface:
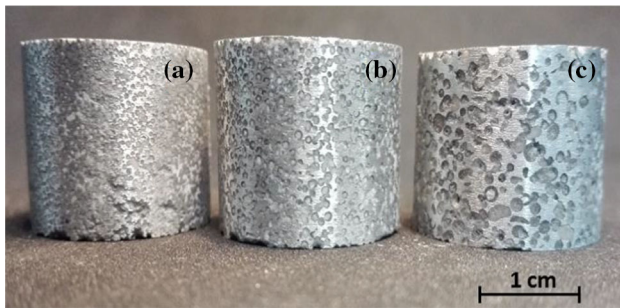

Fig. 6—Photographs of the composites after they were machined. (a) Particles of 496 μm, (b) particles of 687 μm and (c) particles of 945 μm.

Table I. Physical Properties of the Zinalco Foams

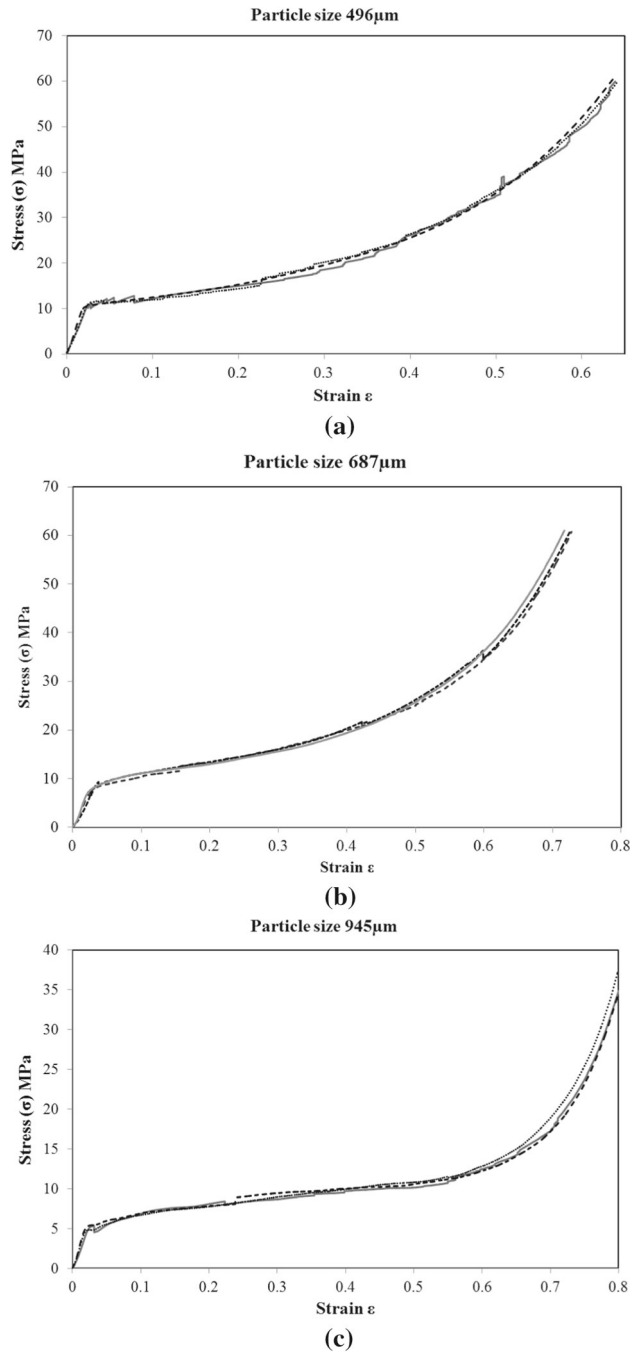| Cell Size Pore (μm)	Sponge Density (kg/m^3)	Relative Density	Porosity (Pct)	Average strut Thickness (μm)
496	2281.86	0.423	58	40
687	2172.56	0.402	60	52
945	1984.64	0.368	63	76

(a)

(b)

(c)

Fig. 7—Compressive stress–strain curves of open-cell Zinalco foams fabricated with particles of (a) 496 μm, (b) 687 μm, (c) and 945 μm.

$$P = \frac{\rho_m \omega^2}{2}\left(r_1^2 - r_0^2\right) \qquad [8]$$

where ρ_m is the density of the molten metal ($\rho_m = 5400$ Kg m^{-3}), ω is the angular velocity ($\omega = 2\pi N$, N is revolution per second), r_1 is the distance from the center of rotation to the inner surface of the preform ($r_1 = 0.275$ m), and r_0 is the thickness of the molten alloy at the beginning of the operation ($r_0 = 0.055$ m). Dimensions of this array can be seen in Figure 8. After several trials from partial infiltration to full infiltration, the
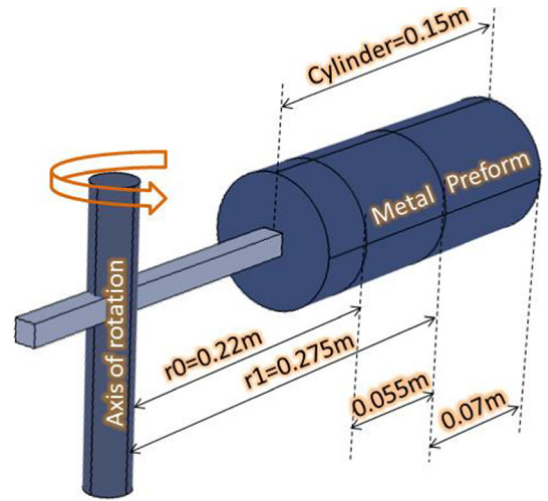

Fig. 8—Schematic drawing of the metal-preform loaded into the rotating mold. Drawing not to scale.

Table II.   Experimental Pressure and Minimum Rotational Speeds

d_f (μm)	$N_{exp.}$ (rev s^{-1})	$P_{exp.}$ (kPa)
496	2.6	18. 137
687	2.0	11.607
945	1.6	7.429

minimum rotational speeds (N) necessary to achieve complete infiltration were determined to be 2.6, 2.0, and 1.7 rev/s for the particle sizes of 496, 687, and 945 μm, respectively. In all the cases, the time investigated was five minutes. Infiltration was repeated three times for each NaCl particle size to ensure the formation of the interrelationship between the rotational speeds and full infiltration. The experimental pressures were deduced using Eq. [8] and are listed in Table II along with their respective particle diameters.

From the data listed in Table II, it can be seen that the pressure necessary to achieve complete infiltration increases as the diameter of the particles decreases. This is expected since the permeability of the preform is proportional to the square of the mean particle diameter ($K \propto d_p^2$). Therefore, as the particle diameter decreases, the permeability diminishes, and more pressure is necessary to overcome the resistance to the filling of the interstitial spaces of the preform with the liquid metal. Eq. [1] shows a linear relationship between the threshold pressure (P_{th}) and the $V_p/[d_p(1 - V_p)]$ term, with a slope of $\gamma Cos\theta$. The latter is the work of immersion defined as the free energy change due to the replacement of the solid-vapor interface by the solid-liquid interface ($\gamma Cos\theta = \sigma_{sv} - \sigma_{sl}$, where σ is the interfacial energy) when immersing the solid in the liquid.[5] To obtain the work of immersion the data for the experimental pressure were plotted as a function of
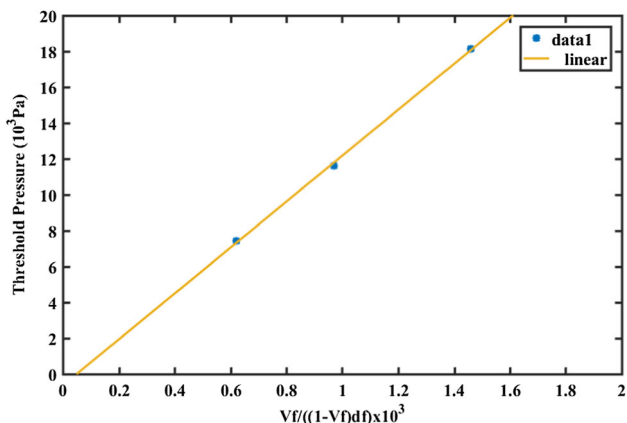
Fig. 9—Experimental results for the threshold pressure for the infiltration of NaCl particles with a Zn-Al-Cu alloy. Linear fitting $R^2 = 0.998$.

Table III. Particle Diameter and Volume Fraction of the Preform

d_p (μm)	V_p	$V_p / [d_p(1 - V_p)] \times 10^3$	P (kPa)
496	0.42	1.459	18. 137
687	0.4	0.970	11.607
945	0.37	0.621	7.429

$V_p / [d_p(1 - V_p)]$ (Figure 9). The values used to obtain the latter term are listed in Table III along with the experimental pressure.

It can be seen in Figure 9 that the data plotted shows a linear relationship. The regression coefficient for the linear fitting is $R^2 = 0.998$, which indicates that the experimental results follow a linear relationship with $V_p / [d_p(1 - V_p)]$. As the capillary law holds (Eq. [1]), this supports the validity of this approach to determine the threshold pressure. From the slope of the fitting line, the work of immersion is computed as $\sigma_{sv} - \sigma_{sl} = \gamma Cos\theta = 2.1$. Because the surface tension of the Zinalco alloy is not yet reported, considering that the main element in the Zinalco alloy is Zinc, we take the surface tension of pure Zn as $\gamma = 0.78$ N/m[37] to size up a value of $\sigma_{sv} - \sigma_{sl} = Cos\theta = 2.1/\gamma$, that is, about 2.7. This factor is comparable with that obtained in,[5] that is 2.9, during the infiltration of fine powders of Al_2O_3, TiC and SiC with pure aluminum, and in,[18] that is 2.6, during the infiltration of Sn-Pb into Al_2O_3, TiC, and SiC preforms. From the linear fitting a straight line is obtained, which corresponds to the threshold pressure:

$$P_{th} = 12.808 \frac{V_p}{d_p(1 - V_p)} - 0.638 [=] Pa \qquad [9]$$

The threshold pressures calculated from Eq. [9] were 18.686, 12.423, and 7.953 kPa for the particle sizes of 496, 687, and 945 μm, respectively. Numerical analysis

of capillarity in packed spheres carried out by Hilden and Trumble[38] shows that the threshold pressure is roughly ten times the infiltrant surface tension, γ, divided by the particle diameter, d_p. Inserting the data of particle diameters and the surface tension value $\gamma = 0.78$ N/m used here in the relationship $(10\gamma/d_p)$, the threshold pressures were calculated to be 15.7 kPa, 11.3 kPa and 8.0 kPa for the particle sizes of 496 μm, 687 μm, and 945 μm, respectively. In the work of Wang et al.,[39] it was observed that to achieve full infiltration, the centrifugal pressure is required to be larger than the flow resistance (Ps) as the particle diameter decreases. The flow resistance was described by the capillary law stated as[39] $P_s = 4\gamma \cos \theta/d_p$. Inserting the data of particle diameters and the value of the work of immersion $\gamma Cos\theta = 2.1$ in the capillary law, the pressures were calculated to be 16.9 kPa, 12.2 kPa, and 8.8 kPa for the particle sizes of 496 μm, 687 μm, and 945 μm, respectively. Although the agreement is quite satisfactory when comparing the values given by Eq. [9] with the values produced by $10\gamma/d_p$ and $(P_s = 4\gamma \cos \theta/d_p)$, we note that the pressure given by Eq. [9] is larger than the pressure calculated using $(10\gamma/d_p)$ and $(P_s = 4\gamma \cos \theta/d_p)$ for the smaller particle size (496 μm), with a maximum difference of 15.5 pct. It is shown that the infiltration of finer pores within a preform does not only depend on the intrinsic wetting parameters, but it is also highly influenced by the narrow interstices between neighboring particles, which act as a scaling parameter on the infiltration pressure required.[6,10,39] Therefore, equations derived from the model of Mortensen et al. (Eq. [1])[4] provide reliable conditions for pressure infiltration, which in turn assist the design of metal foams in a wide range of open pore space in the NaCl packed preform because the equations derived from the model of Mortesen et al[4] are a function of intrinsic wetting parameters and factors of the solid elements such as the particle size and volume fraction. It is shown that using Eq. [9], the threshold pressure to infiltrate Zinalco alloy into NaCl particles for given particle size and volume fraction can be determined.

D. Capillary Infiltration Rates of Zn-Al–Cu Liquid Alloy into NaCl Particles

To validate the value obtained for the work of immersion for the Zinalco alloy/NaCl preform system found in this research, we use Washburn's equation.[29] This equation predicts the rate at which the liquid fills the preform under its capillary pressure or work of immersion (the numerator in the coefficient of penetrance of the liquid $(\gamma \cos \theta/2\eta)$). In the formulation, infiltrated distance, h, increases parabolically in time, t, assuming that infiltration is limited by viscous friction, η.

$$\frac{h^2}{t} = r \frac{\gamma \cos \theta}{2\eta} \qquad [10]$$

here γ is the surface tension, θ is the wetting angle, and r is the effective pore radius. This model has proven its usefulness to predict melt infiltrations for non-reactive systems[40] such as the present metal-salt system. For

reactive infiltration, the model underpredicts the rate of infiltration since the reactive infiltration is limited by the reactive products instead of the viscous flow.[41] Because of lack of data available about wettability properties of the Zinalco (Zn-Al-Cu) ternary alloys, the viscosity η of the alloy was obtained from data of the binary Zn-Al alloy,[42] following the argument that the effects due to the interplay of the different alloying elements are weak, as reported in Reference 43. The value was estimated to be 3.8 mPa s. The effective pore radius is given by the following equation[44,45]:

$$r = \frac{d_p \phi}{6(1 - \phi)} \qquad [11]$$

where d_p is the particle diameter and ϕ is the void fraction. Figure 10 shows the infiltrated distance as a function of the square root of time using the Washburn's equation for the NaCl particle infiltrated with a Zn-Al-Cu liquid alloy under its threshold pressure of 18.137 kPa, 11.607 kPa, and 7.429 kPa for the particle sizes of 496 μm, 687 μm, and 945 μm, respectively. It can be seen that the liquid alloy completely infiltrates the preform of the particles of size 496, 687, and 945 μm in 17, 11, and 7 $s^{1/2}$, respectively. Infiltration proceeds at different rates; the slopes of the linear regression fit lines were 4.1, 6.3, and 9.9 mm/s$^{1/2}$ for the particles of size 496 μm, 687 μm, and 945 μm, respectively. Results show that infiltration rates decrease as the threshold pressure increases. The maximum infiltration time was determined by taking the square of the time (17 $s^{1/2}$), which is 4.8 minutes. This time is consistent with that observed in the experimental trials during infiltration, where complete infiltration was achieved in about five minutes for the particles of size 496 μm. Moreover, to ensure complete infiltration of the foam for the smallest NaCl particle size used, micromechanical modeling of this foam was used as a tool to compare Young's modulus of completely and incompletely infiltrated foam. Young's modulus predictions are compared to the experimental value, as shown in Section III–E. As the infiltration rates were unknown during experimental trials, infiltration
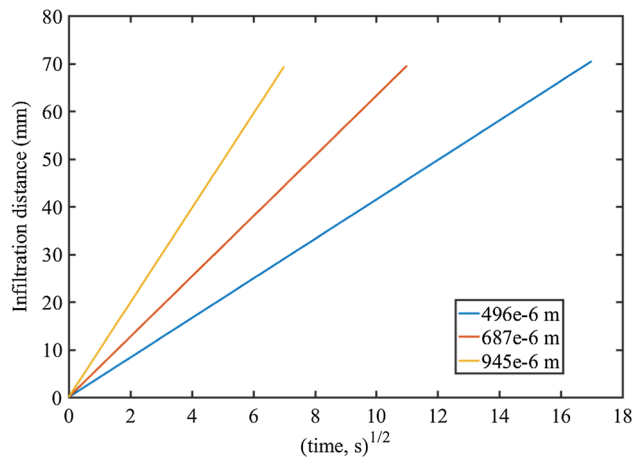
time was arbitrarily established to be five minutes (the mold is held rotating for this time) after which complete infiltration was observed for the smallest particle size studied in this work. From Figure 10, the infiltration times were two minutes and 49 s for the particles of size 687, and 945 μm, respectively. Since the infiltration time observed in the experimental trials for the particles of size 496 μm coincides with the time computed using the Washburn's equation, where infiltration rate is predicted as a function of the work of immersion, the value deduced experimentally of this parameter in this work is validated.

E. Numerical Simulation of Young's Modulus for the Zinalco Foam

During the infiltration process, large interstices of the preform are penetrated by the liquid metal more easily than the smaller ones. For the foams manufactured using the NaCl particles of 687, and 945 μm, whose infiltration times are two minutes and 49 s, respectively, it is clear that complete infiltration is achieved because the experimental time used (five minutes) is larger about two and five times. However, for the foam manufactured using the NaCl particles of size 496 μm the infiltration time in the threshold pressure is essentially the experimental infiltration time used. Therefore, to determine the level of infiltration in this foam, finite element analysis models of the Zinalco foam for the pore size of 469 μm were used as a tool to simulate the elastic behavior of the foam when the foam is fully infiltrated and when the foam is partially infiltrated. Young´s modulus estimations were compared to the experimental value of the foam, which is 0.559 GPa.

Figures 11(a) through (g) show the von Mises stress distribution under compressive deformation (x-direction) for the Zinalco foams when they are infiltrated to the extent of 85, 90, 95, and 100 pct, respectively. Figure 11(b) through (h) show their respective Young's moduli. In Figure 11(a) through (g), it is seen that as the level of infiltration increases, the stress distribution becomes homogeneously distributed among all the struts that make up the cell, which increases the strength of foam. When the foam is not fully infiltrated, the absence of strut connections, as well as the shape variation and uneven cross-sections of the struts in the cell produces inhomogeneous deformation of the lattice, which in turn produces different local stress concentrations. The stress concentration depends on curvature effects present in the foam geometry derived from incomplete replication or incomplete filling of the foam, leading the cellular material to yield at lower values of stress, indicating a reduction in the strength of the foam. Figure 11(b) through (h) show elastic modulus predicted to be 0.29 GPa, 0.44 GPa, 0.49 GPa, and 0.54 GPa when the foam is infiltrated to the extent of 85, 90, 95, and 100 pct, respectively. The experimental value obtained for Young's modulus is 0.559 GPa. Then, the relative error obtained by comparing the elastic modulus of the fully infiltrated foam against the experimental value is lower than 4 pct, which, firstly confirms the validity of the numerical model and secondly confirms that the
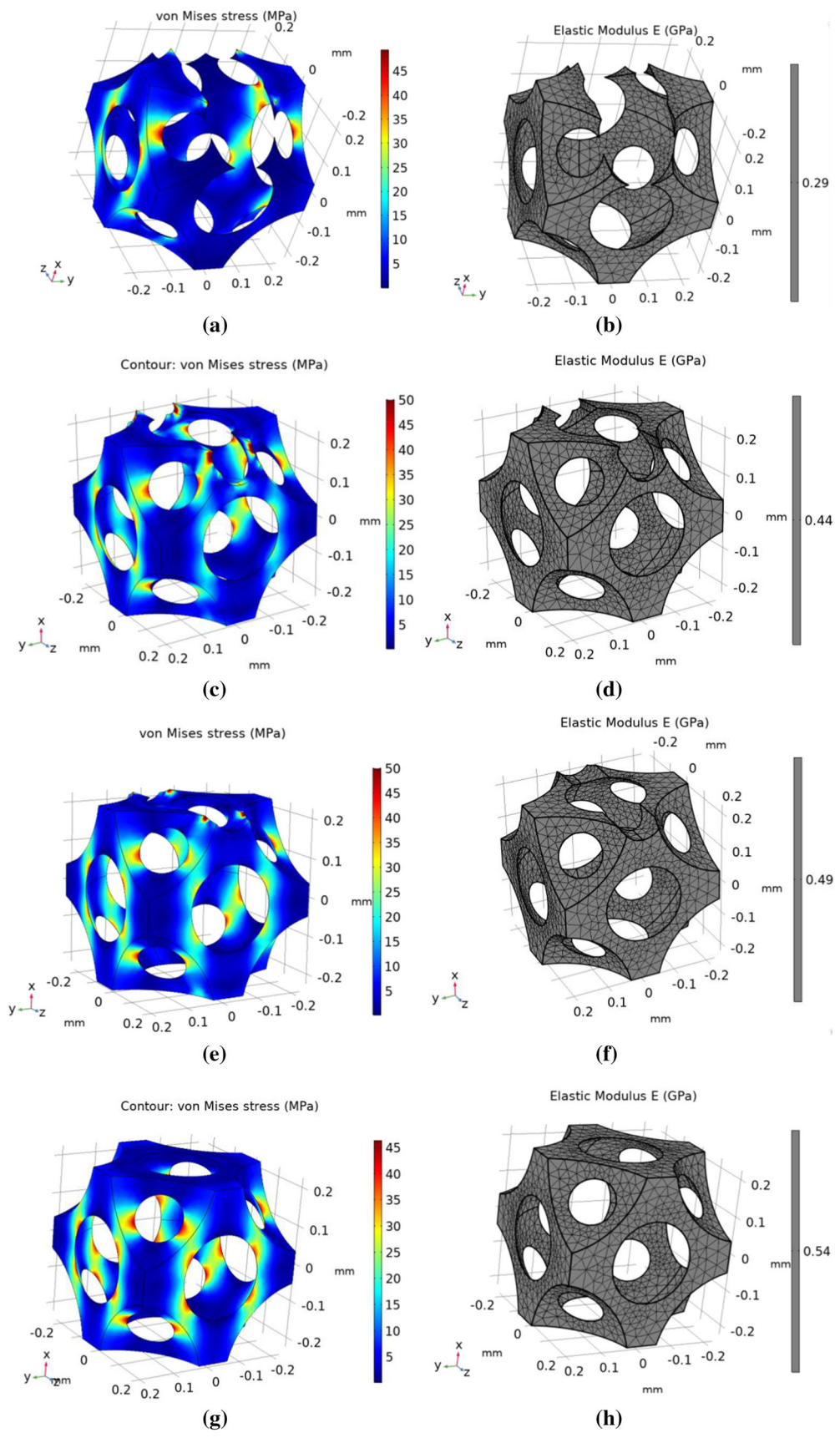

Fig. 10—Infiltrated distance vs square root of time for the NaCl particle infiltrated with a Zn-Al-Cu liquid alloy under the threshold pressure.

Fig. 11—(*a*, *c*, *e*, *g*) von Mises stress distribution in partially and fully infiltrated foam and its corresponding (*b*, *d*, *f*, *h*) Young's moduli.

foam is fully infiltrated, as suggested by the infiltrated distance obtained by the Washburn's equation.[29] Hence, the NaCl preforms with a particle of size 496 μm are properly infiltrated. The elastic modulus of the foam is reduced to about 46 pct when the extent of filling of the foam is only 85 pct because of the absence of load-bearing strut linking nodes in the lattice. It is shown that the mechanical properties such as the strength of the foam depend strongly on the level of infiltration and the foam structure regularity, which depend on the pressure of infiltration. It is shown that equations that allow the prediction of the minimum pressure to achieve complete infiltration (threshold pressure) are useful to obtain better quality in the foams. On the other hand, the comparison between Young's modulus obtained experimentally to the numerical one, shows that infiltration by the centrifugal force in the threshold pressure allows controlling the density of the cellular solid, and the foam structure is relatively neat and regular.

In the current research, it was found that the maximum time needed to achieve complete infiltration of the Zinalco alloy into the NaCl preform (particle size of 496 μm) is 5.8 times larger than the least time (particle size of 945 μm); hence, distinctly different infiltration rates are identified. It is expected that different infiltration durations accompanied by different strut thicknesses based on each particle size affect the microstructure and mechanical properties of cast alloys because they produce different cooling rates during solidification of the metal. Therefore,

thinner cell struts result in a refined microstructure, which in turn produces a stronger strut. Similar dendritic microstructures independent of the strut thickness have been found in the as-produced Zinalco foams in our previous work,[21] as well as other investigations[24,26] unless the Zinalco foams undergo heat treatments once they are produced.[24] Thus, the strength in Zinalco foams as a function of the strut thickness remains to be understood and forms part of this research. Figures 12(a) through (c) shows the von Mises stress distribution under compressive deformation (x - direction) for the Zinalco foams for the particle sizes of 496, 687, and 945 μm, whose average cell-strut thickness were reported in Reference 21 to be 40, 52, and 76 μm, respectively. It is seen in Figure 12 that as the NaCl particle size increases, the cell size, pore size, and the strut thickness of the Zinalco foams increase. Hence, coarse particles on the preform produce thicker and longer struts of the foam. Figures 12(a) through (c) shows that as a result of longer struts in the foam, their bending and buckling resistance is lowered, concentrating the stress in the central strut portion. Then, this stress concentration in the central strut portion forces the foam to yield at lower values of stress, which results in lower strength and hence a lower elastic modulus of the foam, as shown in Figures 12(d) through (f). Elastic numerical moduli are 0.54, 0.36, and 0.23 GPa, for the foams with cell sizes of 496, 687, and 945 μm, respectively. On the other hand, fine particles produce thinner and shorter struts in the foam; in turn, shorter struts increase their resistance to
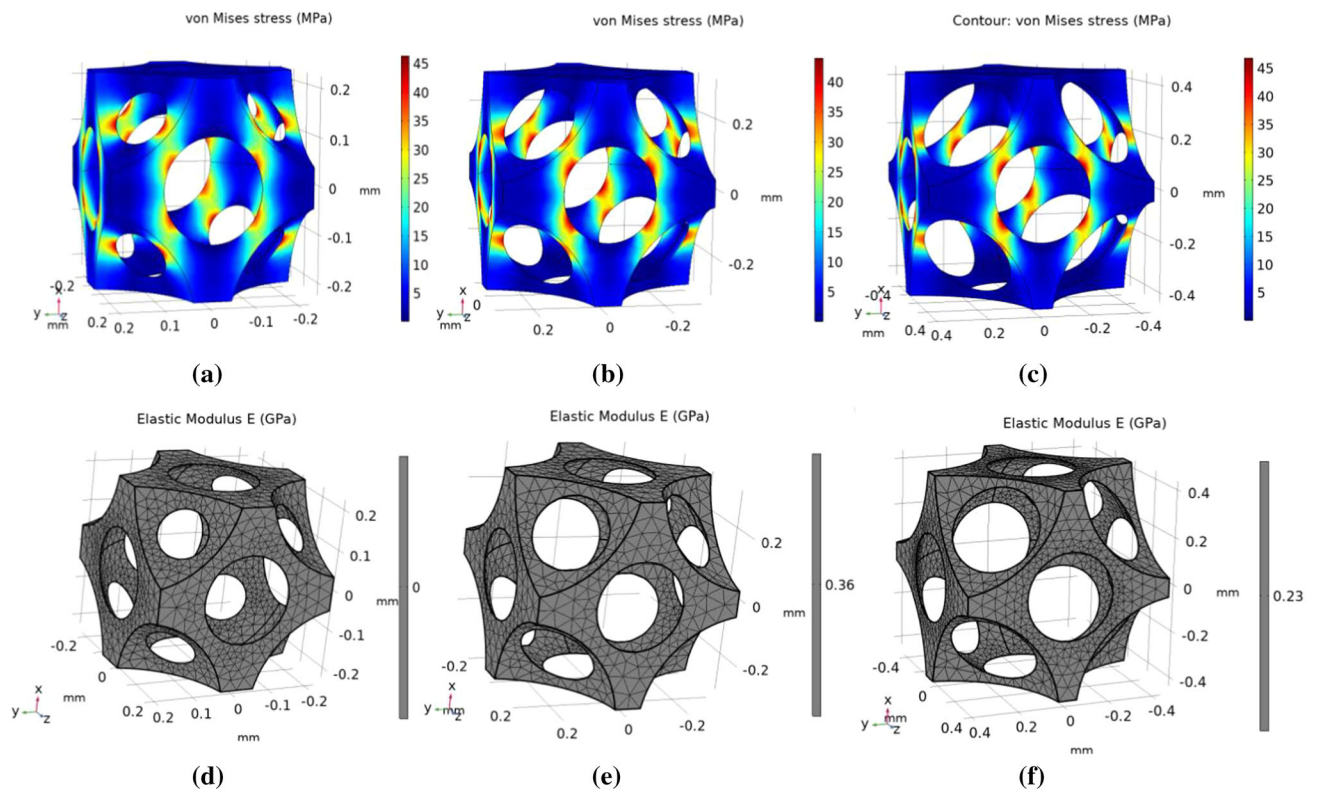

Fig. 12—(*a* to *c*) von Mises stress distribution in fully infiltrated foam and its (*d*, *e*, *f*) corresponding Young's moduli. Experimental elastic moduli are 0.559 GPa, 0.35 GPa, and 0.234 GPa for the foams with cell sizes of 496, 687, and 945 μm, respectively.

bending. Hence, its ability to resist elastic deformation in the foam is increased. These results show that the elastic properties of the as-produced Zinalco foams are governed by structural parameters such as the pore size and the strut length, which depend on the salt particle size.

IV. CONCLUSIONS

This work investigated the infiltration of Zinalco alloy into NaCl packed particle using a simple centrifugal experimental setup. The threshold pressure, which increases as the particle size decreases, was deduced experimentally. The work of immersion was determined from the threshold pressure. An equation to predict the threshold pressure to infiltrate Zinalco alloy into NaCl circular particles for given particle size and volume fraction was established, which can be used to aid the design of preform structures for this porous medium/infiltrant system. The value of the work of immersion is 2.1, which was validated by studying the infiltration rates by employing Washburn's equation. The factor $\cos\theta/\gamma$ is about 2.7, which compares very well to the range of 2.6 to 2.9 reported in the literature, obtained during the infiltration of fine powders of Al_2O_3, TiC and SiC with pure Al and Sn-Pb. Results show that infiltration rates decrease as the threshold pressure increases, and infiltration proceeds at different rates for particles of size 496, 687, and 945 μm. The comparison in terms of Young's modulus of the foam for the smallest cell size, and the predictions of the micromechanical models shows that complete infiltration is achieved in the foams under the experimental pressure applied; therefore, the equation to predict the threshold pressure is relievable. Moreover, the numerical results show that as the level of infiltration increases, the stress in the produced foams gets homogeneously distributed among all the struts that make up the cell, which increases the strength of foam. The elastic properties of the as-produced Zinalco foams are governed by structural parameters such as the pore size and the strut length. Coarse particles in the preform produce thicker and longer struts of the foam. Consequently, their bending and buckling resistance is lowered, concentrating the stress in the central strut portion. This stress concentration in the central strut portion forces the foam to yield at lower values of stress, which results in lower strength and hence a lower elastic modulus of the foam. Fine particles produce thinner and shorter struts in the foam; in turn, shorter struts increase their resistance to bending. Hence, the foam's ability to resist elastic deformation is increased.

REFERENCES

1. A. Sutygina, U. Betke, and M. Scheffler: *Mater*, 2019, vol. 12, pp. 1–12.
2. A. Sutygina, U. Betke and M. Scheffler: *Adv. Eng. Mater*, 2020, pp. 1–8.
3. C. Gaillard, J.F. Despois, and A. Mortensen: *Mater. Sci. Eng*, 2004, vol. 374, pp. 250–62.
4. A. Mortensen and J. Cornie: *Metall. Trans. A*, 1987, vol. 18, pp. 1160–63.
5. A. Alonso, A. Pamies, J. Narciso, C. Garcia-Cordovilla, and E. Louis: *Metall. Trans. A*, 1993, vol. 24, pp. 1423–32.
6. J.F. Despois, A. Marmottant, L. Salvo, and A. Mortensen: *Mater. Sci. Eng A*, 2007, vol. 462, pp. 68–75.
7. B. Soni and S. Biswas: *J. Mater. Res*, 2018, vol. 33, pp. 3418–29.
8. T. Yamauchi and Y. Nishida: *Acta. Metall. Mater*, 1995, vol. 43, pp. 1313–21.
9. E. Luna, E.M., Barari, F., Woolley, R., Goodall, R: 2014, *J. Vis. Exp.* (94), e52268, pp. 1–12.
10. Y. Conde, J.F. Despois, R. Goodall, A. Marmottant, L. Salvo, C. San Marchi and A. Mortensen: *Adv. Eng. Mater*, 2006, vol. 8, pp. 795–803.
11. Y. Nishida, I. Shirayanagi, and Y. Sakai: *Metall. Trans. A*, 1996, vol. 27, pp. 4136–39.
12. J. Wannasin and M.C. Flemings: *J. Mater. Process. Technol*, 2005, vol. 169, pp. 143–49.
13. B. Xiong, H. Yu, Z. Xu, Q. Yan, and C. Cai: *J. Alloys Compd*, 2011, vol. 509, pp. 279–83.
14. R. Etemadi, B. Wang, K.M. Pillai, B. Niroumand, E. Omrani, and P. Rohatgi: *Mater. Manuf. Process*, 2018, vol. 33, pp. 1261–90.
15. D.J. Britnell and K. Neailey: *J. Mater. Process. Technol.*, 2003, vol. 138, pp. 306–10.
16. S. Rajagopal and W.H. Altergott: *AFS Trans*, 1985, vol. 93, pp. 145–54.
17. G.C. Manjunath Patel, P. Krishna and M.B. Parappagoudar: *Adv. Automob. Eng*, 2015, vol. 4, pp. 1–9.
18. J. Wannasin and M.C. Flemings: *Scr. Mater.*, 2005, vol. 53, pp. 657–61.
19. X. Huang, C. Liu, X. Lv, G. Liu, and F. Li: *J. Mater. Process. Technol.*, 2011, vol. 211, pp. 1540–46.
20. G. Chirita, D. Soares, and F.S. Silva: *Mater. Des.*, 2008, vol. 29, pp. 20–27.
21. A. Sánchez, A. Cruz, J.E. Rivera, J.A. Romero, M.A. Suárez, and V.H. Gutiérrez: *Metall. Trans. A*, 2018, vol. 49, pp. 272–281.
22. Z. Wang, J. Gao, K. Chang, L. Meng, N. Zhang, and Z. Guo: *RSC adv.*, 2018, vol. 8, pp. 15933–15939.
23. A. Jinnapat and A. Kennedy: *Met*, 2011, vol. 1, pp. 49–64.
24. S. Casolco, G. Dominguez, D. Sandoval, and J.E. Garay: *Mater. Sci. Eng. A*, 2007, vol. 471, pp. 28–33.
25. D.P. Mondal, M.D. Goel, Niharika Bagde, Nidhi Jha, Sonika Sahu, A.K. Barnwal: *Mater. Des.*, 2017, vol. 57, pp. 315–24.
26. Y. Siron, J. Liu, M. Wei, X. Zhu, and Y. Liu: *Mater. Des.*, 2009, vol. 30, pp. 87–90.
27. C. Gaillard, J.F. Despois, and A. Mortensen: *Mater. Sci. Eng. A*, 2004, vol. 374, pp. 250–62.
28. D.W. Huo, J. Yang, X.Y. Zhou, H. Wang, and T.K. Zhang: *Nonferrous Met. Soc. China*, 2012, vol. 22, pp. 85–89.
29. E.W. Washburn: *Phys. Rev*, 1921, vol. 17, pp. 273–83.
30. J. Hinojosa-Torres and J.M. Aceves-Hernández: *Orient. J. Chem*, 2012, vol. 3, pp. 1147–52.
31. J.E. Rivera-Salinas, K.M. Gregorio-Jáuregui, J.A. Romero-Serrano, A. Cruz-Ramírez, E. Hernández-Hernández, A. Miranda-Pérez, and V.H. Gutierréz-Pérez: *Met*, 2020, vol. 10, pp. 1–19.
32. J. C. Carranza, L. Pérez R. Ganesan, B. Y. Casas, R. A. L. Drew, C. Ruiz-Aguilar, I. A. Figueroa and I. Alfonso: *J. Braz. Soc. Mech. Sci. Eng*, 2019, vol. 41 pp. 1–8.
33. H.X. Zhu, J.F. Knott, and N.J. Mills: *J. Mech. Phys. Solids*, 1997, vol. 45, pp. 319–43.

34. W.E. Warren and A.M. Kraynik: *J. Appl. Mech*, 1988, vol. 55, pp. 341–46.
35. Y.X. Gan, C. Chen, and Y.P. Shen: *Int. J. Solids Struct*, 2005, vol. 42, pp. 6628–42.
36. R. Guerra Silva, U. Teicher, A. Brosius and S.Ihlenfeldt: *Mater,* 2020, vol. 13, pp. 1–15.
37. R.L. Guthrie: *Engineering in Process Metallurgy*, Clarendon Press, Oxford, 1990.
38. J.L. Hilden and K.P. Trumble: *J. Coll. Interf. Sci.*, 2003, vol. 267, p. 463.
39. Z. Wang, J. Gao, K. Chang, L. Meng, N. Zhang, and Z. Guo: *RSC Adv.*, 2018, vol. 8, pp. 15933–39.
40. S.J. Glass and D.J. Green: *J. Am. Ceram. Soc*, 1999, vol. 82, pp. 2745–52.
41. Eo. Einset: *J. Amer. Ceram. Soc,* 1996, vol. 79, pp. 333–38.
42. V.M.B. Nunes, M.J.V. Lourenço, F.J.V. Santos, and C.A. Nieto de Castro: *Int. J. Thermophys.*, 2010, vol. 31, pp. 2348–60.
43. J. Goicoechea, C. Garcia-Cordovilla, E. Louis, and A. Pamies: *Mater. Sci.*, 1992, vol. 27, pp. 5247–52.
44. S.Y. Oh, J.A. Cornie, and K.C. Russell: *Metall. Trans. A.*, 1989, vol. 20, pp. 527–32.
45. P.B. Maxwell, G.P. Martins, D.L. Olson, and G.R. Edwards: *Metall. Trans. B*, 1990, vol. 21, pp. 475–85.